NUKLEONIKA 2007;52(3):125–131

ORIGINAL PAPER

Gamma-ray computed tomography as a tool to evaluate porosity changes along depth for surface crusted soils

Luiz F. Pires,
Osny O. S. Bacchi,
Klaus Reichardt,
Nivea M. P. Dias

Abstract. Assessment of changes in porosity (ϕ) along depth for soils with surface crusting is difficult because conventional soil physical investigation tools are destructive and usually require a long period of time for preparation and analysis of the samples. Computed tomography (CT) has frequently been used as a method to evaluate soil structure in a non-destructive, sensitive, and rapid manner. CT data can be used for measuring at a millimetric scale changes in ϕ along depth for soils with surface crusting. The main objective of this work was to investigate the sensibility of the gamma-ray CT to assess soil structural changes along depth in samples presenting structural crust. CT images were taken with a first generation scanner of 1.14 mm resolution along eight different soil layers within the 0–28 mm depth. Porosity increased along depth up to the 14–17.5 mm layer. Through the analysis of the ϕ distribution of each layer it was possible to show that the sealed surface layer presented ϕ values of approximately 30%, while the other layers were greater than 30% up to 60% (macropore regions). The sealing crust thickness was estimated to be in the range of 2.3–3.5 mm.

Key words: gamma-ray attenuation • soil density • soil structure • soil surface sealing • ^{241}Am • applied nuclear physics • gamma tomography

Luiz F. Pires✉
Department of Physics,
State University of Ponta Grossa, UEPG,
C. E. P. 84.030-900, Ponta Grossa, PR, Brazil
and Center for Nuclear Energy in Agriculture,
The University of São Paulo,
C. P. 96, C. E. P. 13.400-970, Piracicaba, SP, Brazil,
Tel.: 55 42 3220 3044, Fax: 55 42 3220 3042,
E-mail: luizfpires@gmail.com and lfpires@uepg.br

O. O. S. Bacchi, K. Reichardt
Center for Nuclear Energy in Agriculture,
The University of São Paulo,
C. P. 96, C. E. P. 13.400-970, Piracicaba, SP, Brazil

N. M. P. Dias
Department of Soil Science,
State University of Ponta Grossa, UEPG,
C. E. P. 84.030-900 Ponta Grossa, PR, Brazil

Received: 14 May 2007
Accepted: 4 July 2007

Introduction

Computed tomography (CT) was first developed for clinical purposes in nuclear medicine and several advances have occurred in the last decades in this scientific field. The rapid growth in all forms of CT can be attributed mainly to more sophisticated computers capable to acquire and store large amounts of data and provide a simple and straightforward means of analysis of these data. CT is a non-destructive inspection technique that, in agronomy, could be an interesting alternative to reliably determine physical deformations of the structure of a soil sample due to natural or anthropogenic activities. This technique allows measurements of soil porosity point to point on a micrometric/millimetric scale without interfering with the physical integrity of the sample. CT technique was first introduced into soil science to evaluate soil bulk density [23], and therefore, the application of CT to evaluate soil structure has been largely discussed in the literature [4, 14, 22, 24, 28].

According to Baver *et al.* [3], the sealing of the soil surface is a specific physical modification. It is a result of the impact of raindrops on bare soils, mainly after soil preparation operations, or during the initial growth stages of the crop, promoting the dispersion of the clay in a soil suspension of high clay and silt content. On

top of the impact energy, the wetting of the drops disintegrates aggregates by mass expansion and explosion of trapped air, following the dispersion and orientation of the finest particles, which infiltrate along with water, plugging pores [11, 16]. During the drying process fine hard layers are formed. When dry they are very compacted, hard, breakable and plain. The crust formed represents a thin cover of approximately 0.1 up to 20 mm [10], and of permeabilities 2000 times less, in comparison to the layer below. A second layer is formed just below the first, made by particles that are carried by the water and that plug pores, with permeabilities 200 times less in comparison to the soil below that is not affected [17]. The relation between macro and microporosity is altered, with predominance of the microporosity, therefore, decreasing soil permeability to water and air. The agronomic disadvantages of soil surface sealing are, mainly, the difficulty for seed germination and the reduction of infiltration rates. The time for surface flooding is reduced, increasing run-off volume, favoring laminar and furrow erosions [27].

Soil compaction causes important modifications on soil structure such as changes in soil porosity, which is related to soil water and gas movement. In a general way it is known that compaction affects soil hydraulic properties, such as decreases in saturated water content, increases in air entry suction, and decrease in saturated hydraulic conductivity and infiltrability [2]. Information about the structural crust of a soil is very important for its characterization, mainly of its hydraulic properties. Some authors [10, 21] have observed the impact of crusting on soil porosity and its variation from the surface down, discussing the impact of crusting on some hydraulic parameters.

This study investigates the sensibility of the gamma-ray computed tomography technique as a method to assess the structural changes along depth for a Brazilian soil presenting structural crust, and to evaluate its thickness.

Material and methods

Soil sampling

Core samples were collected in 2006 in a coffee field from the surface layer of a soil characterized as Eutric Nitosol (Ne) (24% sand, 33% silt, 43% clay, 20.2 $g \cdot kg^{-1}$ organic matter, 1.62 $g \cdot cm^{-3}$ dry bulk density) in Piracicaba, SP, Brazil (22°4' S; 47°38' W; 580 m a.s.l.). According to Koppen's classification the climate is of the Cwa type, tropical highland, mesothermal with dry winter. Average values for air temperature, rainfall, and relative humidity are 21.2°C; 1.253 mm per year; and 74%, respectively. The dry season covers June-August, July being the driest month. During spring-summer, October to March, very high intensity rainfall events are common, several of them reaching 50 mm per hour or more. Six cylindrical samples (h = 3.0 cm, D = 4.8 cm, $V \approx 55$ cm^3) were collected from the soil surface layer with aluminum cylinders using a stainless steel core sampler (3.2 cm high and 5.0 cm in internal diameter to allow the introduction of the aluminum cylinder). The sampler was inserted into the soil by impact, with a rubber hammer falling from a fixed height, as traditionally done. After complete insertion of the aluminum cylinders into the soil, the surrounding soil was carefully removed to minimize further soil disturbance due to vibration, shear stress, and compaction. The excess of soil at the bottom surface was carefully trimmed off and made flat to be sure that the soil volume was approximately equal to the internal volume of the soil.

Instrumentation and experimental set-up

The CT scanner was a first-generation system with a fixed source-detector arrangement and translation/rotational movements of the samples (Fig. 1). The radioactive gamma-ray source consisted of ^{241}Am (59.54 keV) with an activity of 3.7 GBq. A NaI(Tl) scintillation crystal (7.62 × 7.62 cm) coupled to a photomultiplier tube was used to detect the monoenergetic photons passing through circular lead collimators (1 mm) mounted between source and detector. Samples were rotated over 180° in intervals of 2.25°, with linear movement intervals of 0.14 cm. The acquired data were stored in a PC and CT images were obtained using the reconstruction algorithm Microvis [20] developed by Embrapa Agricultural Instrumentation Center (CNPDIA) located in São Carlos, SP, Brazil. Voxel size obtained was $1.14 \times 1.14 \times 1.00$ mm^3. Calibration of the system was made on the basis of the linear regression between linear attenuation coefficients (μ) and tomographic units (TU) of various homogeneous materials [22]. TU is linearly related to a unit called Hounsfield unit (HU). Water is used as a reference medium for HU (for water, HU = 0), while the reference medium for TU is air with its minimal μ value. In the case of a soil, TU is a result of the contributions from solid mineral and organic components, water, and air, which makes the coefficient of attenuation different for each path of the beam through the sample. Attenuation of the beam by the air is insignificant as compared with the attenuation by soil particles and water, and can, therefore, be neglected.

A contrast transfer function (CTF) was used to evaluate the quality of the tomographic images [6]. To eliminate possible artifacts, the area in an image selected for the analysis was smaller than the whole sample section covered by CT analysis, as had been suggested previously [13]. With this approach, the portions of the samples adjacent to the cylinder walls were excluded, since there the abrupt density changes (from soil to aluminum) might have produced image distortions.

Data analysis

The soil bulk density (ρ_b) was calculated by substituting the angular coefficient of the linear regression between μ (cm^{-1}) and TU and mass attenuation coefficients of water and soil, respectively, in the Beer-Lambert equation. The following equation was derived to obtain ρ_b ($g \cdot cm^{-3}$) [22]:

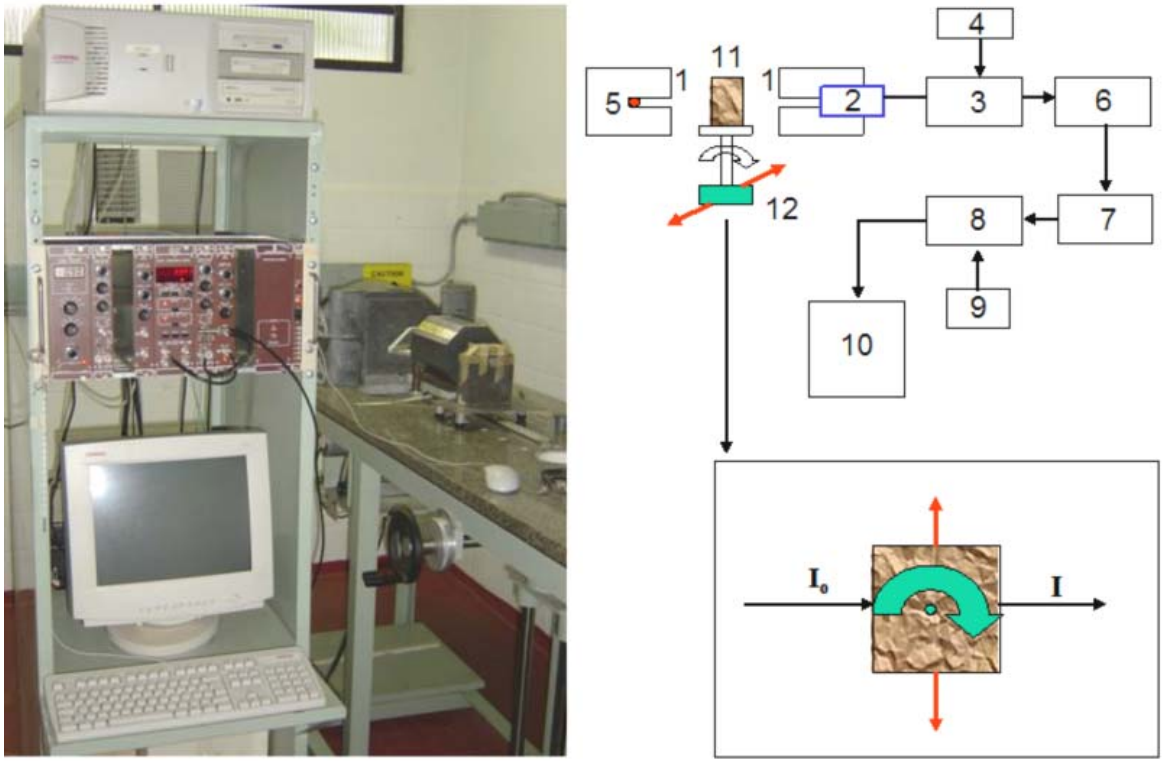

Fig. 1. (A) View of the first generation computed tomography (CT) system with the respective electronics. (B) Schematic diagram of the CT system: 1 – lead collimators; 2 – NaI(Tl) detector; 3 – photomultiplier; 4 – high-voltage unit; 5 – ^{241}Am source; 6 – amplifier; 7 – single-channel analyzer; 8 – counter; 9 – timer; 10 – PC; 11 – soil sample; 12 – rotation-translation system I_o and I, are, respectively, the rates of the incident and the emerging photon beams.

$$\rho_b = \left[\left(\frac{TU}{997.72}\right) - (0.199\theta)\right] \Big/ 0.328 \quad (1)$$

where θ ($cm^3 \cdot cm^{-3}$) represents the air dry volumetric soil water content of the sample before CT scanning.

The measurement of the soil sample porosity was made using the following equation:

$$\phi = \left(1 - \frac{\rho_b}{\rho_p}\right) \cdot 100 \quad (2)$$

where ϕ represents the percent total porosity and ρ_p is the soil particle density. Details about the method used to measure ρ_p can be found in Flint and Flint [9]. Eight different soil layers (0–3.5 mm (L1); 3.5–7.0 mm (L2); 7.0–10.5 mm (L3); 10.5–14.0 mm (L4); 14.0–17.5 mm (L5); 17.5–21.0 mm (L6); 21.0–24.5 mm (L7), 24.5–28.0 mm (L8)) were selected for the evaluation of ϕ variation with depth. Each layer represents an arithmetic ϕ mean value of three layers with approximately 1.2 mm each.

For the evaluation of μ_s air-dried soil was passed through a 2.0 mm sieve and packed into a thin wall acrylic container ($10 \times 10 \times 10$ cm^3). The intensities of monoenergetic photons were measured at 20 different positions in the soil sample, the linear attenuation coefficient representing an arithmetic mean of these measurements.

The SAS software [29] was employed for data processing. An analysis of variance (ANOVA) and Duncan test (at $\alpha = 0.05$) were performed to analyze statistical differences and to discriminate means.

Results and discussion

The mass attenuation coefficients for the Eutric Nitosol (Ne) and water were 0.328 ± 0.003 and 0.199 ± 0.003 $cm^2 \cdot g^{-1}$, respectively, for the 59.54 keV photons, which agree with values found in the literature for ^{241}Am sources [1, 8]. The slope of the linear regression between μ and TU was 0.998 cm; the correlation coefficient r^2 was 0.999. This high correlation coefficient was essential for obtaining high-quality soil images. The average ρ_p obtained for four replicates of the Ne was 2.68 ± 0.01 $g \cdot cm^{-3}$, which agree with values found in the literature for clayey soils [12].

Figure 2 shows a CT image of a soil sample of the Ne that presents a sealed layer at the upper surface. The planes of image acquisition were vertical and the available data permitted a continuous 2-D analysis of TU distributions and, consequently, of ϕ variations along the sample.

By image analysis of Fig. 2 data, it is possible to observe qualitatively that the lowest ϕ values in relation to the whole sample, are located at the upper surface layer, confirming the existence of a crust sealing process in the soil surface region. At the bottom of the sample

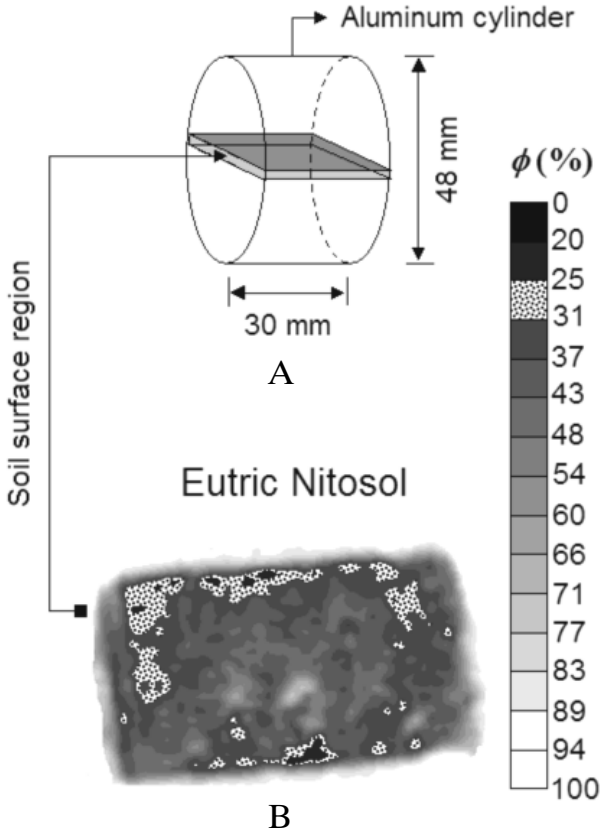

Fig. 2. (A) Schematic diagram of the region ($30 \times 48 \times 1$ mm^3) used for computed tomographic image analysis. (B) Tomographic image of a soil sample with surface crusting. The scale represents the soil porosity (ϕ) distribution, where white and black areas represent macropores and stones, respectively.

there is a small region with low ϕ values, which probably were induced by the procedure of sample preparation for CT scanning, once the excess of soil at the bottom surface was carefully trimmed off and made flat with a blade.

The distributions of soil porosity along depth for each selected layer of the CT soil image presented in Fig. 2 are shown in Fig. 3, in which ϕ for each layer (soil sample thickness) is represented by the height of the bar.

As it can be seen from Fig. 3, the configuration of the ϕ distribution presents significant changes in the upper 3.5 mm (Fig. 3a) when compared with the other layers. The upper dense crust layer (L1) practically shows a homogeneous distribution of ϕ with average values of 30%. The total porosity configuration for the 3.5 to 14.0 mm layers (Figs. 3b to 3d) changes little, showing an increase of several ϕ average values near or beyond 40% along histogram positions. L5 and L6 (Figs. 3e and 3f) also present similar ϕ configuration, but different from the first four layers. The presence of two visible peaks with ϕ average values greater than 50%, like the positions 15 and 23 in Fig. 3e and 14 and 22 in Fig. 3f is related to the presence of a large hole in the soil sample (see white regions in Fig. 2). For L7 (Fig. 3g), it is possible to observe two ϕ average values greater than 50% (located at positions 24 and 25 from the left border of the cylinder) due to the macropore inside the sample and four ϕ average values of approximately 30% (located at positions 14 and 15 and 39 and 40 from the left border of the cylinder) due to the sealing caused by the compaction during sample preparation. Soil porosity in L8 (Fig. 3h) presents some peaks (located at positions 9, 19, 30, and 37 from the left border of the cylinder) due to the existence of some small macropores near the bottom surface of the soil sample. It is possible to observe for all analyzed layers (Fig. 3) that practically the lowest ϕ average values are located close to the extremes (region near the edge of the samples inside the cylinder) of histograms. This result was confirmed by Pires *et al.* [25] that evaluated the influence of sampling in soil structure, showing a density gradient from the center to the edge of samples indicating a clear tendency of compaction near the edges. Other authors [4, 28] also have investigated the effect of sampling volume in measurements of soil physical properties.

Figure 4 shows absolute ϕ average values for each layer, which represent an arithmetic mean of six replicates.

In Fig. 4 the increase of soil porosity is non linear with the greatest increase of ϕ in relation to another analyzed layer occurring for L2. Similar results were reported by Fox *et al.* [10] working with a sandy loam soil from Canada. The upper dense crust (L1) shows the lowest ϕ average values in relation to the other layers, confirming the existence of a sealed region at the soil surface. Epstein and Grant [7] have attributed the reduction of the porosity in a sealed region to the compaction of the surface by raindrop impact. Soil porosity changes little beyond L3 to L6; although the changes in ϕ are statistically significant ($\alpha = 0.05$) between L3–L4 and L5–L6. On the other hand, the differences of ϕ are not significant between L3 and L4 and L5 and L6. Soil porosity presents a tendency of decrease for L7 and L8, which probably occurred due to the procedure of sample preparation as previously discussed. If L7 and L8 are eliminated of our analysis the increase of ϕ can be adjusted through the following equation $y = 3.81Ln(x) + 28.76$ ($r^2 = 0.98$). Through this mathematical adjustment it could be possible to define a transition zone for the sample with crust. Below the upper dense crust (L1), L2 appears to be a transition zone. This zone presents an increase in the number of positions (Fig. 3b) with ϕ average values greater than 30%. Values of ϕ near 30% (Fig. 3a) are characteristic of a dense crust region. It is important to have in mind that information about changes in soil porosity with depth can be helpful for the estimation of hydraulic parameters in crust infiltration models [5, 10, 18] and to define a transition zone to better evaluate the sealing crust region.

Through 2-D tomographic images it was possible to estimate the sealing crust thickness that varied from 2.3 to 3.5 mm. Pires *et al.* [26] found a variation of 2 to 4 mm for the sealing crust thickness of a clayey soil submitted to sewage sludge application. Fox *et al.* [10] evaluated a crust thickness of 5 mm for a sandy loam soil. Macedo *et al.* [15] through microtomography analysis of undisturbed soil samples submitted to

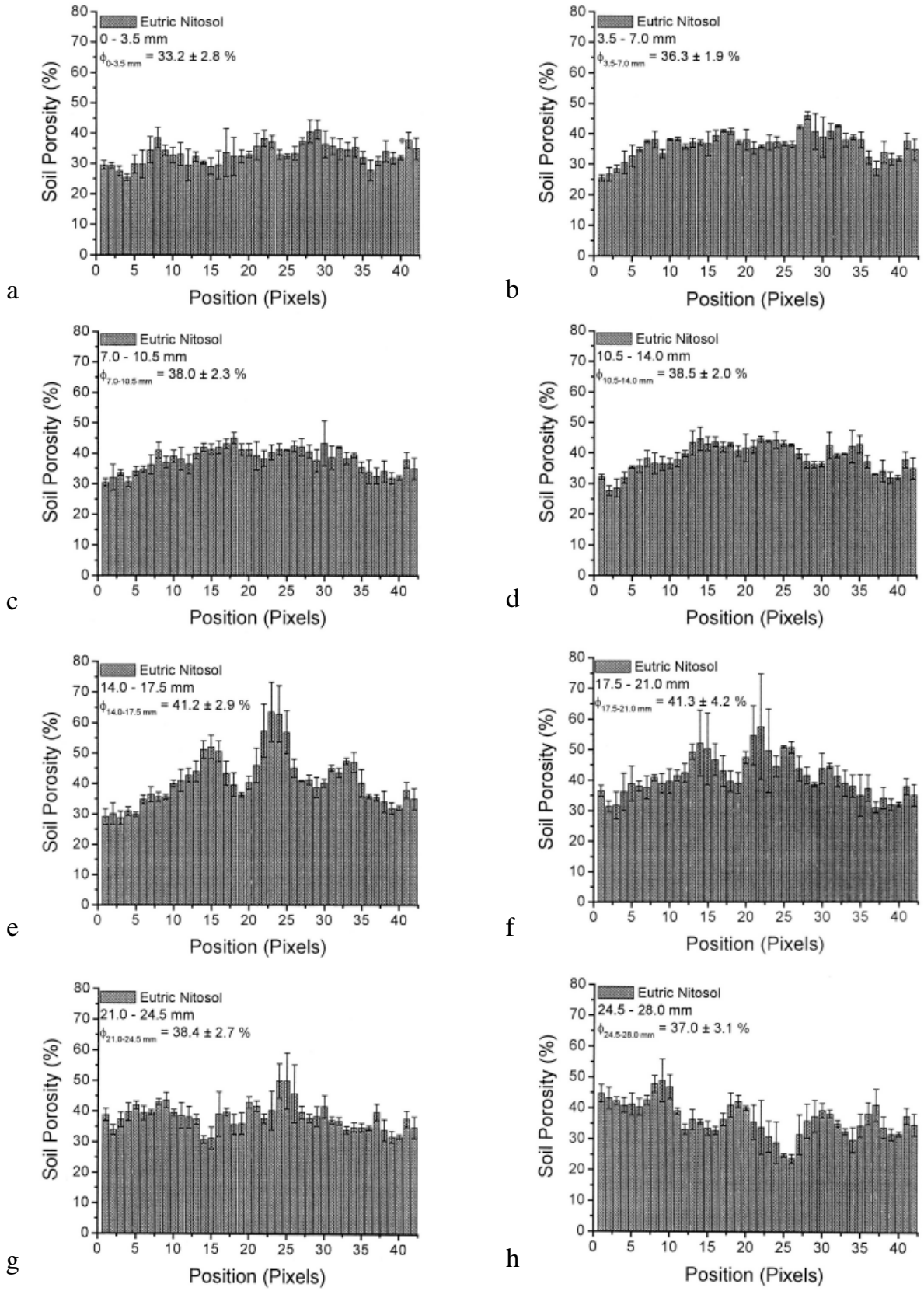

Fig. 3. Distribution of the soil porosity with position (soil width) for each analyzed layer.

irrigation determined a crust thickness of 0.5 mm caused by the raindrop impact. According to Wu and Fan [30] there are positive correlation relationships between the raindrop intensity and the compactness and thickness of surface crusts. Mees and Singer [19] working with undisturbed samples of different types of surface crusts from soils of the southern Aral Sea basin found a variation of 5 to 30 mm for the crust thickness.

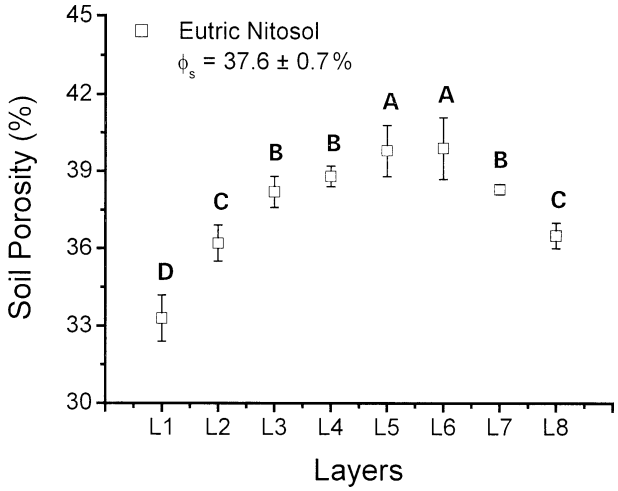

Fig. 4. Variations in the soil porosity with depth for each analyzed layer (0–3.5 mm (L1); 3.5–7.0 mm (L2); 7.0–10.5 mm (L3); 10.5–14.0 mm (L4); 14.0–17.5 mm (L5); 17.5–21.0 mm (L6); 21.0–24.5 mm (L7); 24.5–28.0 mm (L8)). Soil porosity data followed by the same letters under each ϕ value in the graphic are not significantly different according to the Duncan test ($\alpha = 0.05$). The statistical analysis was applied within layers (errors bars are 95% confidence intervals).

Concluding remarks

The CT is a valuable non-destructive inspection technique that allows detailed analysis of soil porosity profiles and the detection of very thin compacted layers of soils with structural crusts. Using 2-D tomographic images it was possible to confirm the occurrence of soil surface sealing, to analyze soil structure changes with depth, and to evaluate the thickness of the sealed layer for a Brazilian clayey soil. These results can provide insights for infiltration models that estimate hydraulic parameters in soils with sealing.

Nomenclature

CT – computed tomography
h – soil sample height, cm
D – soil sample diameter, cm
V – soil sample volume, cm^3
PC – personal computer
CTF – contrast transfer function
L – soil layer, mm
r^2 – correlation coefficient
Ne – Eutric Nitosol
TU – tomographic unit
HU – Hounsfield unit
μ_m – mass attenuation coefficient, $cm^2 \cdot g^{-1}$
μ – linear attenuation coefficient, cm^{-1}
μ_s – soil linear attenuation coefficient, cm^{-1}
ρ_b – soil bulk density, $g \cdot cm^{-3}$
ρ_p – soil particle density, $g \cdot cm^{-3}$
θ – soil water content, $cm^3 \cdot cm^{-3}$
ϕ – soil porosity, %

Acknowledgment. The authors are grateful to Fundação Araucária (Grants no. 10193 and 10195), Fundo Paraná/SETI, Governo do Estado do Paraná, and CNPq for the financial support.

References

1. Appoloni CR, Rios EA (1994) Mass attenuation coefficients of Brazilian soils in the range 10–1450 keV. Appl Radiat Isot 45:287–291
2. Assouline S, Tavares-Filho J, Tessier D (1997) Effect of compaction on soil physical and hydraulic properties: experimental results and modeling. Soil Sci Soc Am J 61:390–398
3. Baver LD, Gardner WJ, Gardner WR (eds) (1973) Física de suelos. Union Tipográfica Editorial Hispano Americana, Mexico
4. Baveye P, Rogasik H, Wendroth O *et al.* (2002) Effect of sampling volume on the measurement of soil physical properties: simulation with X-ray tomography data. Meas Sci Techn 13:775–784
5. Cousin I, Malam Issa O, Le Bissonnais Y (2005) Micro-geometrical characterization and percolation threshold evolution of a soil crust under rainfall. Catena 62:173–188
6. Cruvinel PE, Cesareo R, Crestana S *et al.* (1990) X- and γ-ray computerized minitomograph scanner for soil science. IEEE Trans Instrum Meas 39:745–750
7. Epstein E, Grant WJ (1973) Surface crust formation as affected by raindrop impact. In: Hadas A (ed.) Physical aspects of soil water and salts in ecosystems. Springer Verlag, Berlin, pp 194–201
8. Ferraz ESB, Mansell RS (1979) Determining water content and bulk density of soil by gamma ray attenuation methods. IFAS, Florida
9. Flint AL, Flint LE (2002) The solid phase: particle density. In: Dane JH, Topp GC (eds) Methods of soil analysis: Part 4. Physical methods. Book Series, vol. 5. Soil Sci Soc Am, Madison, pp 229–240
10. Fox DM, Bryan RB, Fox CA (2004) Changes in pore characteristics with depth for structural crusts. Geoderma 120:109–120
11. Fox DM, Le Bissonnais Y, Quétin P (1998) The implications of spatial variability in surface seal characteristics for infiltration in a mound and depression microtopography. Catena 32:101–114
12. Grohmann F (1960) Distribuição do tamanho de poros em tres tipos de solos do Estado de São Paulo. Bragantia 19:319–328
13. Herman GT (ed.) (1980) Image reconstruction from Projections. Academic Press, London
14. Jégou D, Brunotte J, Rogasik H *et al.* (2002) Impact of soil compaction on earthworm burrow systems using X-ray computed tomography: preliminary study. Soil Biol 38:329–336
15. Macedo A, Crestana S, Vaz CMP (1998) X-ray micro-tomography to investigate thin layers of soil clod. Soil Till Res 49:249–253
16. McIntyre DS (1958a) Soil splash and the formation of surface crusts by raindrop impact. Soil Sci 85:261–266
17. McIntyre DS (1958b) Permeability measurements of soil crusts formed by raindrop impact. Soil Sci 85:185–189
18. Malam Issa O, Cousin I, Le Bissonnais Y, Quétin P (2004) Dynamic evolution of the unsaturated hydraulic conductivity of a developing crust. Earth Surf Process Landforms 29:1131–1142
19. Mees F, Singer A (2006) Surface crusts on soils/sediments of the southern Aral Sea basin, Uzbekistan. Geoderma 136:152–159

20. Microvis (2000) Programa de Reconstrução e Visualização de Imagens Tomográficas, Guia do Usuário. EMBRAPA/CNPDIA, São Carlos, Brasil
21. Mualem Y, Assouline S, Rohdenburg H (1990) Rainfall induced soil seal (A): a critical review of observations and models. Catena 17:185–203
22. Pedrotti A, Pauletto EA, Crestana S *et al.* (2005) Evaluation of bulk density of Albaqualf soil under different tillage systems using the volumetric ring and computerized tomography methods. Soil Till Res 80:115–123
23. Petrovic AM, Siebert JE, Rieke PE (1982) Soil bulk density analysis in three dimensions by computed tomographic scanning. Soil Sci Soc Am J 46:445–450
24. Phogat VK, Aylmore LAG (1989) Evaluation of soil structure by using computer-assisted tomography. Aust J Soil Res 27:313–323
25. Pires LF, Bacchi OOS, Reichardt K (2004) Damage to soil physical properties caused by soil sampler devices as assessed by gamma ray computed tomography. Aust J Soil Res 42:857–863
26. Pires LF, Macedo JR, Souza MD *et al.* (2002) Gamma-ray computed tomography to characterize soil surface sealing. Appl Radiat Isot 57:375–380
27. Pla I (1985) A routine laboratory index to predict the effects of soil sealing on soil and water conservation. In: Proc of the Symp on the Assessment of Soil Surface Sealing and Crusting, Ghent, Belgium, pp 154–162
28. Rogasik H, Onasch I, Brunotte J *et al.* (2003) Assessment of soil structure using X-ray computed tomography. In: Mees F, Swennen R, van Geet M, Jacobs P (eds) Applications of X-ray computed tomography in the geosciences. Special Publications, vol. 215. Geological Society, London, pp 151–165
29. SAS Institute (1996) System for information. Version 6.11. Cary, SAS Institute Inc.
30. Wu FQ, Fan WB (2002) Analysis on factors affecting soil crust formation on slope farmland. J Soil Water Conserv 16:33–36